J. Appl. Comput. Mech., 11(2) (2025) 451-466
DOI: 10.22055/jacm.2024.46464.4532

ISSN: 2383-4536
jacm.scu.ac.ir

Shahid Chamran University of Ahvaz

Journal of Applied and Computational Mechanics

Research Paper

Bond-Slip Model for Finite Element Analysis of Reinforced Recycled Aggregate Concrete Frames

Worathep Sae-Long[1], Suchart Limkatanyu[2], Nattapong Damrongwiriyanupap[1], Piti Sukontasukkul[3], Tanakorn Phoo-Ngernkham[4], Thanongsak Imjai[5], Suraparb Keawsawasvong[6]

[1] Department of Civil Engineering Program, School of Engineering, University of Phayao, Phayao, 56000, Thailand, Email: worathep.sa@up.ac.th (W.S.L.); nattapong.da@up.ac.th (N.D.)

[2] Department of Civil and Environmental Engineering, Faculty of Engineering, Prince of Songkla University, Songkhla, 90112, Thailand, Email: suchart.l@psu.ac.th

[3] Construction and Building Materials Research Center, Department of Civil Engineering, King Mongkut's University of Technology North Bangkok, Bangkok, 10800, Thailand, Email: piti.s@eng.kmutnb.ac.th

[4] Sustainable Construction Material Technology Research Unit, Department of Civil Engineering, Faculty of Engineering and Technology, Rajamangala University of Technology Isan, Nakhon Ratchasima 30000, Thailand, Email: tanakorn.ph@rmuti.ac.th

[5] School of Engineering and Technology, Walailak University, Nakhorn Si Thammarat, 80160, Thailand, E-mail: thanongsak.im@wu.ac.th

[6] Research Unit in Sciences and Innovative Technologies for Civil Engineering Infrastructures, Department of Civil Engineering, Faculty of Engineering, Thammasat School of Engineering, Thammasat University, Pathumthani, 12120, Thailand, Email: ksurapar@engr.tu.ac.th

Received March 27 2024; Revised July 05 2024; Accepted for publication August 24 2024.
Corresponding author: N. Damrongwiriyanupap (nattapong.da@up.ac.th)

Abstract. The use of coarse recycled aggregate in structural concrete members is an alternative and beneficial way to reduce the consumption of natural materials. This is not only due to the limitation of resources of aggregates, but also due to the sustainability of concrete that can make construction industry more eco-friendly and consequently mitigate the global warming. The bond between recycled aggregate and reinforcing steel bars is one of the key factors that is interesting and significant in terms of the design and safety of reinforced concrete structures. Therefore, this paper develops and introduces a novel bond-slip model and frame element incorporating the bond-slip effect to analyze recycled aggregate concrete (RAC) structures under static loads. The proposed frame model is built on the Euler-Bernoulli kinematics beam theory and employs a fiber-discrete section model derived from the displacement-based formulation. Uniaxial material models are utilized to capture the nonlinear behaviors of RAC frames reinforced with steel bars. The bond-slip model is developed and refined through regression analysis of available experimental data on pull-out failure, enabling the assessment of bond interface slip between RAC and deformed bars. To validate the accuracy and efficiency of the proposed frame model, two numerical simulations are studied. The first simulation investigates the accuracy and convergence of the proposed model, while the second examines the impact of the bond-slip interface on the response analysis of RAC beams. Both simulations emphasize the significance of the bond-slip interface in analyzing RAC frame systems.

Keywords: Recycled aggregate concrete, Bond-slip model, Euler-Bernoulli beam, Reinforced concrete frames, Finite element, Fiber-section model.

1. Introduction

The utilization of alternative materials in engineering structures has become increasingly interesting and important in recent years [1-3]. Recycled materials, in particular, have gained popularity due to their potential to reduce waste and impact on the environment. [4-5]. Numerous recycled materials have been currently investigated for their suitably used as sustainable and durable construction materials [6-11]. For instance, Maurya et al. [6] conducted a study on the utilization of recycled glass to enhance concrete properties. Ou et al. [7] used recycled waste slag in producing synchronous grouting materials for the applications in tunneling engineering. Im et al. [8] explored the performance and engineering properties of recycled asphalt shingles (RAS) and reclaimed asphalt pavement (RAP) mixed with hot-mix asphalt for pavement applications. Julphunthong et al. [9] investigated the utilization of calcium carbide residue and coal fly ash as alternative binders to enhance the compressive strength of pastes and mortars for soil stabilization purposes. Additionally, the use of recycled concrete aggregate (RCA) as coarse aggregate to evaluate the mechanical properties of recycled aggregate concrete (RAC) was carried out by Damrongwiriyanupap et al. [10] and Monika et al. [11]. Among these recycled materials, RCA has gained significant interest in engineering applications [12-15], primarily due to its widespread availability from the demolition of reinforced concrete buildings [11, 16]. Therefore, this highlights the importance of studying the mechanical properties and applications of RCA in engineering fields and is an urgent task for further promoting the adoption of sustainable construction materials in the future.

Published online: August 30 2024

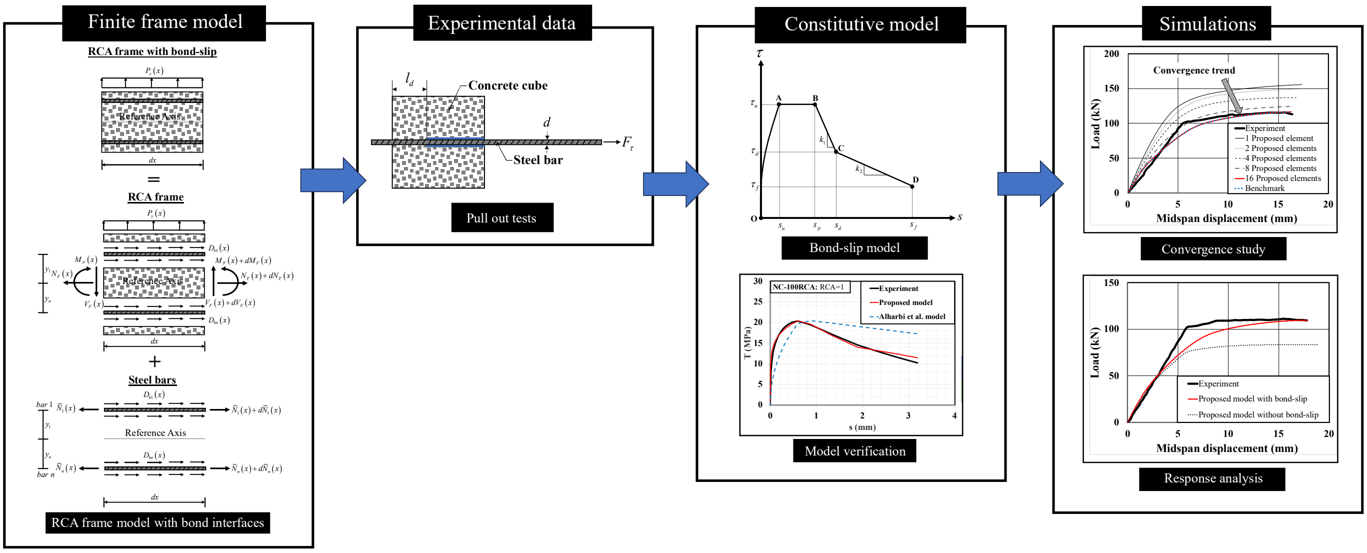

Fig. 1. Schematic configuration of research frameworks.

In construction involving RAC, there are many issues have been investigated; such examples include the mechanical properties related to the replacement ratio of RCA in mixtures [17-20], the bond-interface between RAC and steel bars [21-22], the quality of coarse aggregate mixes [23], durability [24], shrinkage [25], and beyond. Within this field of studies [17-25], particular emphasis is placed on the bond-interface effect, which has critical importance in structural analysis, particularly in reinforced RAC structures. This effect concerns the interaction between reinforcing steel bars and the surrounding RAC matrix, exerting a substantial influence on load and shear transfer, structural behaviors, and flexural capacity [26-28]. A comprehensive understanding of bond interface behavior between RAC and reinforcing steel is required for ensuring safe and effective utilization. Consequently, extensive research has been dedicated to this area [29-38]. For instance, Xiao and Falkner [29] investigated on bond behavior between RAC and steel rebars via 36 pullout tests, considering various percentage of RCA replacement and two types of steel rebar. Their findings highlighted a decrease in bond strength with increasing amount of RCA replacement, while the bond strength between RAC and plain rebar remained consistent. Additionally, Kim et al. [30] evaluated bond behavior in high-strength concrete mixed with RCA, comparing different substitution ratios and reinforcing bar types. The study revealed that bond stress and slip relation in RAC had minimal influence on bar arrangement direction, location, and substitution rate. Li et al. [31] carried out the pull-out test of 24 full-recycled-aggregate concrete (aRAC) specimens with deformed steel bars, examining the impact of aRAC strength, bond length, and lateral constructional stirrups on bond behavior, and proposed a bond-slip relationship. Furthermore, Kim et al. [33] investigated bond behavior between RAC and deformed steel rebars, focusing on recycled coarse aggregate replacement ratio (RCAr) and water-to-cement ratio, establishing a linear relationship between bond strength and RCA density. They also developed a multivariable model for predicting RAC bond strength using these parameters, demonstrating good prediction of RAC degradation characteristics. Subsequent studies by Kim et al. [33] is the assessment of bond behavior between deformed steel rebars and RAC through pull-out tests, revealing a decrease in maximum bond strength and an increase in slip with increased aggregate water absorption. Further investigations reported by Guerra et al. [34] examined the impact of replacing natural coarse aggregates by recycled concrete coarse aggregates on the anchorage strength of ribbed steel rebars to concrete. Prince et al. [35] conducted thirty pullout tests on 8- and 10-mm deformed steel bars embedded in RAC, exhibiting higher normalized bond strengths across all RCA replacement percentages when compared to natural coarse aggregate concrete. Additionally, Wardeh et al. [36] presented experimental results on 96 concrete pullout specimens made with natural and recycled aggregates using deformed steel bars, revealing bond strength and failure mechanisms closely aligned, with values exceeding Eurocode 2 predictions. Abdulazeeza et al. [37] examined the bond strength behavior of a deformed steel bar embedded in RAC using experimental and numerical analysis, finding a 13% reduction in bond strength compared to conventional concrete, with similar failure modes. Lastly, Su et al. [38] investigated the bond behavior of RAC with steel bars, revealing that failure modes are influenced by various factors such as steel bar diameter, concrete cover to diameter ratio, and RCA replacement ratio, which affected the load-slip curve. From these studies [29-38], it is evident that the bond-interface slip of RAC is complex and dependent on numerous parameters, emphasizing its significance in engineering design.

In order to characterize the bond-interface slip between RAC and reinforcing bars within RAC structures, it is necessary to develop bond strength models and bond-slip constitutive laws. This necessity has motivated several works to propose such models [29, 31, 35, 39], as noted by Su et al. [38]. For instance, Xiao and Falkner [29] introduced a bond-slip relation between RAC and steel bars with two empirical parameters for finite element analysis of RAC members. This model showed a balance between simplicity and accuracy, making it widely adopted for predicting bond-interface behavior in RAC members [33, 35, 36]. Subsequently, Prince et al. [35] simplified the bond-slip constitutive model of Xiao and Falkner [29] and proposed a new bond-slip relationship with only one parameter. However, this model failed to capture the softening response adequately. Following this, Cao et al. [39] presented a three-stage model for RAC and reinforcing steel bars, including the residual region, while Li et al. [31] proposed a four-stage model based on the least squares approach, accounting for micro-slip, slip, internal splitting-broken, and decline segments. Despite the accuracy and simplicity of these bond constitutive models, they largely rely on empirical parameters that are challenging to define and may not be suitable for engineering applications and practices. Hence, there is still room for improvement and development of these bond-slip constitutive models for finite element analysis of RAC structures, motivating the study presented in this work.

The primary objective of this study is to introduce a novel frame model incorporating the bond-interface slip effect for analyzing RAC structures. This proposed model is formulated based on the displacement-based approach within the framework of Euler-Bernoulli beam theory. To subdivide the frame cross-section, we employ the fiber-section model [26], while employing uniaxial material models to represent the behavior of each constituent material in the RAC member, including the RAC model, reinforcing steel model, and proposed bond-interface slip model. The RAC model is adapted from the concrete model presented by Kent and Park [40], and the reinforcing steel model follows the model developed by Menegotto and Pinto [41]. The bond-slip model is developed and tailored from the bond-slip model between concrete and steel bars, originally proposed by Limkatanyu and Spacone

[27, 42], using regression analysis [43]. Thus, this study presents, a novel fiber-section frame model incorporating the bond-slip effect for analyzing RAC members. Two numerical simulations are conducted to evaluate the model's accuracy and demonstrate the influence of the bond-slip effect on the response analysis of RAC structures. These simulations are performed employing the general-purpose finite element platform FEAP [44].

2. Schematic Configuration of Research Frameworks

To present the research framework of this paper, a schematic configuration is shown in Fig. 1. The first stage involved deriving the finite frame model based on the displacement-based formulation. Three essential components for the structural analysis were identified: equilibrium equations, compatibility equations, and constitutive relations. In the subsequent step, experimental data from pull-out tests of RAC and steel bars were collected from the literature. These data were then utilized to develop and propose the bond-slip constitutive law for RAC and reinforcing steel. Subsequently, this bond-slip model was employed to investigate the response of RAC beams under static loads. Two numerical simulations were conducted: one is to validate the accuracy of the model and the other is to examine the impact of the bond-slip effect.

3. Finite Element Analysis of RAC Frame: Displacement-Based Formulation

The finite element analysis (FEA) is a computational method used to explore the behavior of physical systems under various conditions and is widely used in engineering applications [45-47]. For example, Ling et al. [45] optimized the wire arc additive manufacturing (WAAM) process using a numerical tool based on FEA, while Imran et al. [46] investigated the fretting wear behavior of steel wire ropes in coal mine technology. A three-dimensional finite element (FE) model was created using ABAQUS and UMESHMOTION comparing results with experimental data. Ghannadi et al. [47] used FEA to discuss the importance of early defect detection in engineering structures due to the increasing complexity of structures. They proposed using a semi-rigidly connected frame element (S-RCFE) instead of the standard Euler-Bernoulli beam element to assemble the experimental beam and establish a high-fidelity numerical model. For the proposed model, the basic contributions of the FE model can be expressed as follows:

3.1. Equilibrium

In the case of reinforced RAC frame elements with bond interfaces, the free body diagram of an infinitesimal segment *dx* of the RAC frame with n bond interfaces is considered, as illustrated in Fig. 2. Based on the small deformation assumption, all equilibrium equations are formulated in the undeformed configuration. The axial equilibrium of the RAC frame with a reinforcing steel bar *i* can be expressed as follows [42]:

- Axial equilibrium of the RAC frame:

$$\frac{dN_F(x)}{dx} + \left(\sum_{i=1}^{i=n} D_{bi}(x)\right) = 0 \tag{1}$$

- Axial equilibrium of the reinforcing steel bar *i*:

$$\frac{d\bar{N}_i(x)}{dx} - D_{bi}(x) = 0 \qquad (\text{for } i = 1, n) \tag{2}$$

where $N_F(x)$ is the axial force in the RAC frame; $D_{bi}(x)$ denotes the bond-interface force between the RAC frame and steel bar *i*; and $\bar{N}_i(x)$ represents the axial force in reinforcing steel bar *i*. It is important to emphasize that the bond-interface slip is considered only in the axial component of the frame. Furthermore, the dowel action in the steel bars is neglected, following the works of Limkatanyu and Spacone [27, 42].

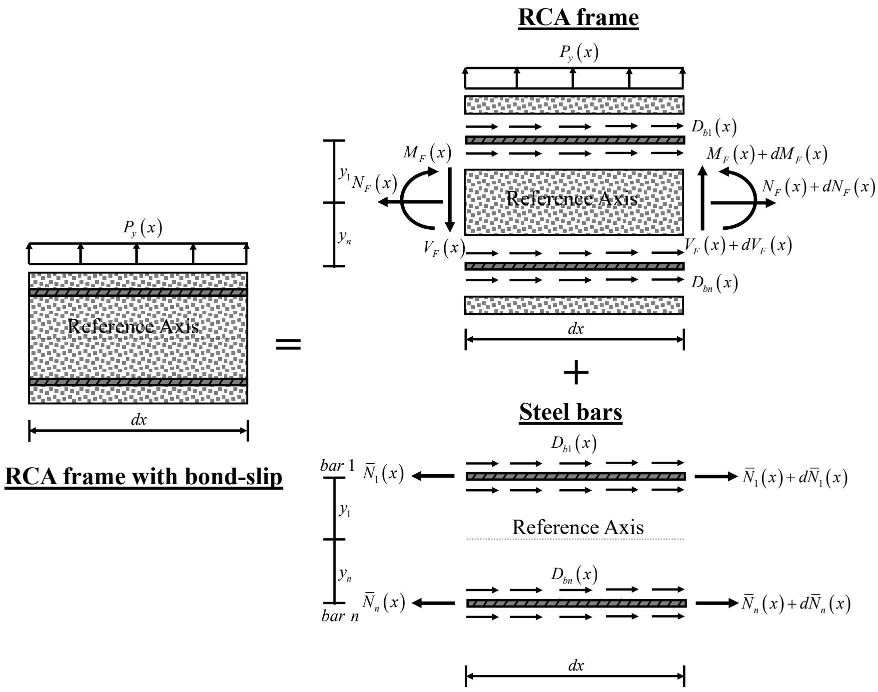

Fig. 2. Free body diagram of an infinitesimal segment of RAC frame with *n* bond-interfaces.

Consider the transverse equilibrium of the infinitesimal segment *dx* of the RAC frame with n bond interfaces, which yields the following equations [42]:

$$\frac{dV_F(x)}{dx} - p_y(x) = 0 \tag{3}$$

where $V_F(x)$ is the shear force in the RAC frame; and $p_y(x)$ denotes the transverse distributed load.

The moment equilibrium of the infinitesimal segment *dx* of the RCA frame with n bond interfaces can be written as [42]:

$$\frac{dM_F(x)}{dx} - V_F(x) - \left(\sum_{i=1}^{i=n} y_i D_{bi}(x)\right) = 0 \tag{4}$$

where $M_F(x)$ represents the bending moment in the RAC frame; and y_i is the distance measured from the reference axis to the bond interface between the RAC frame and steel bar *i*, as plotted in Fig. 2.

Based on the Euler-Bernoulli beam theory, the shear force $V_F(x)$ can be eliminated out from Eq. (4) by differentiating Eq. (4) with respect to *x* and substituting Eq. (3) into Eq. (4), leading to the following equation [42]:

$$\frac{d^2M_F(x)}{dx^2} - p_y(x) - \left(\sum_{i=1}^{i=n} y_i \frac{dD_{bi}(x)}{dx}\right) = 0 \tag{5}$$

For sake of simplifying the equilibrium equations of Eqs. (1), (2), and (5), it can be rewritten in matrix form as [42]:

$$\mathbf{L}^T\mathbf{D}(\mathbf{x}) - \mathbf{L}_b^T\mathbf{D}_b(\mathbf{x}) - \mathbf{p}(\mathbf{x}) = \mathbf{0} \tag{6}$$

in which

$$\begin{aligned} \mathbf{D}(\mathbf{x}) &= \left\{\mathbf{D}_F(\mathbf{x}) \ \vdots \ \bar{\mathbf{D}}(\mathbf{x})\right\}^T \\ \mathbf{D}_b(\mathbf{x}) &= \left\{D_{b1}(x) \ \cdots \ D_{bn}(x)\right\}^T \\ \mathbf{p}(\mathbf{x}) &= \left\{0 \ \ p_y(x) \ \ 0 \ \cdots \ 0\right\}^T \end{aligned} \tag{7}$$

where $\mathbf{D}_F(\mathbf{x}) = \left\{N_F(x) \ \ M_F(x)\right\}^T$ represents the frame-section force vector; $\bar{\mathbf{D}}(\mathbf{x}) = \left\{\bar{N}_1(x) \ \cdots \ \bar{N}_n(x)\right\}^T$ stands for the bond-interface force vector; $\mathbf{L}$ and $\mathbf{L}_b$ are the differential operators and can be defined as [42]:

$$\mathbf{L} = \begin{bmatrix} \frac{d}{dx} & 0 & \vdots & 0 & 0 & 0 \\ 0 & \frac{d^2}{dx^2} & \vdots & 0 & 0 & 0 \\ \cdots & \cdots & \cdots & \cdots & \cdots & \cdots \\ 0 & 0 & \vdots & \frac{d}{dx} & \cdots & 0 \\ 0 & 0 & \vdots & 0 & \cdots & 0 \\ 0 & 0 & \vdots & 0 & \cdots & \frac{d}{dx} \end{bmatrix}; \text{ and } \mathbf{L}_b = \begin{bmatrix} -1 & y_1\frac{d}{dx} & 1 & 0 & 0 \\ \cdots & \cdots & \cdots & \cdots & \cdots \\ -1 & y_n\frac{d}{dx} & 0 & 0 & -1 \end{bmatrix} \tag{8}$$

It is interesting to note that the number of unknown internal forces in the system is 2*n*+2, whereas there is only *n*+2 equilibrium equations available. Consequently, the RAC frame system can be categorized as internally statically indeterminate. The determination of internal forces solely from the equilibrium equations is not feasible.

3.2. Compatibility

The compatibility equations give the correlation between deformations and displacements at any section of the RAC frame and bond interfaces. In the RAC frame, the deformation vector $\mathbf{d}(\mathbf{x})$ is formed as the conjugate work pair of the force vector $\mathbf{D}(\mathbf{x})$ and can be represented as follows [42]:

$$\mathbf{d}(\mathbf{x}) = \left\{\mathbf{e}_F(\mathbf{x}) \ \vdots \ \bar{\mathbf{e}}(\mathbf{x})\right\}^T \tag{9}$$

where $\mathbf{e}_F(\mathbf{x}) = \left\{\varepsilon_F(x) \ \ \kappa_F(x)\right\}^T$ denotes the frame-section deformation vector, containing the axial strain $\varepsilon_F(x) = du_F(x)/dx$ and the bending curvature $\kappa_F(x) = d^2v_F(x)/dx^2$; $\bar{\mathbf{e}}(\mathbf{x}) = \left\{\bar{\varepsilon}_1(x) \ \cdots \ \bar{\varepsilon}_n(x)\right\}^T$ is the bond-interface deformation vector, containing the axial strain of the *n* bars with bond interface $\bar{\varepsilon}_i(x) = d\bar{u}_i(x)/dx$; $u_F(x)$ and $v_F(x)$ represent the axial and transverse frame displacements; and $\bar{u}_i(x)$ is the axial displacement of the *n* bars with bond interface.

The section displacements can be written in matrix form as [42]:

$$\mathbf{u}(\mathbf{x}) = \left\{\mathbf{u}_F(\mathbf{x}) \ \vdots \ \bar{\mathbf{u}}(\mathbf{x})\right\}^T \tag{10}$$

where $\mathbf{u}_F(\mathbf{x}) = \left\{u_F(x) \ \ v_F(x)\right\}^T$ is the frame-section displacement vector; and $\bar{\mathbf{u}}(\mathbf{x}) = \left\{\bar{u}_1(x) \ \cdots \ \bar{u}_n(x)\right\}^T$ is the bond-interface displacement vector.

The compatibility equations for the frame can be expressed in the matrix form as [42]:

$$\mathbf{d}(\mathbf{x}) = \mathbf{L}\mathbf{u}(\mathbf{x}) \tag{11}$$

According to the works of Limkatanyu and Spacone [27, 42], the compatibility relationship between bond-interface slips and frame displacements of the generic bars *i* yields [42]:

$$u_{bi}(x) = \bar{u}_i(x) - u_F(x) + y_i \frac{dv_F(x)}{dx} \tag{12}$$

where $u_{bi}(x)$ represents the relative bond-interface slip between the frame section and steel bar i. The compatibility equations of the bond interface can be explained in matrix form as [42]:

$$\mathbf{d}_b(\mathbf{x}) = \mathbf{L}_b \mathbf{u}(\mathbf{x}) \tag{13}$$

where $\mathbf{d}_b(\mathbf{x}) = \{u_{b1}(x) \quad \cdots \quad u_{bn}(x)\}^T$ is the bond-interface deformation vector.

Equations (11) and (13) describe the compatibility relations for the RAC frame member with n bond interfaces. In addition, it is notable that there exists a contragradient nature between the equilibrium equation in Eq. (6) and the compatibility relations in Eqs. (11) and (13) as revealed by the differential operators.

3.3. Constitutive Relations

The nonlinearity inherent in the proposed frame model with bond interfaces arises from the nonlinear force-deformation relations, which are dependent on each material model. Consequently, the sectional force within the frame and bond-interface force can be expressed as the functions of sectional deformations [42]:

$$\mathbf{D}(\mathbf{x}) = \Psi[\mathbf{d}(\mathbf{x})] \quad \text{and} \quad \mathbf{D}_b(\mathbf{x}) = \Omega[\mathbf{d}_b(\mathbf{x})] \tag{14}$$

In the scenario of a linear elastic material system, Eq. (14) can be explicitly written as [42]:

$$\mathbf{D} = \mathbf{k}_F \mathbf{d} \quad \text{and} \quad \mathbf{D}_b = \mathbf{k}_b \mathbf{d}_b \tag{15}$$

where $\mathbf{k}_F$ denotes the RAC frame stiffness matrix; and $\mathbf{k}_b$ is the bond-interface stiffness matrix.

In the context of Euler-Bernoulli beam theory, the stiffness matrices for the RAC frame section and bond interfaces are described as follows [42]:

$$\mathbf{k}_F = \begin{bmatrix} \int_A E_F dA & 0 & \vdots & 0 & \cdots & 0 \\ 0 & \int_A y^2 E_F dA & \vdots & 0 & \cdots & 0 \\ \cdots & \cdots & \cdots & \cdots & \cdots & \cdots \\ 0 & 0 & \vdots & E_{s1}A_{s1} & \cdots & 0 \\ \cdots & \cdots & \vdots & \cdots & \cdots & \cdots \\ 0 & 0 & \vdots & 0 & \cdots & E_{sn}A_{sn} \end{bmatrix} \quad \text{and} \quad \mathbf{k}_b = \begin{bmatrix} E_{b1}\rho_{b1} & \cdots & 0 \\ \cdots & \cdots & \cdots \\ 0 & \cdots & E_{bn}\rho_{bn} \end{bmatrix} \tag{16}$$

where E_F and A represent the modulus of elasticity and area of the RAC frame, respectively; y is the distance measured from the neutral axis to the centroid of each considered fiber; E_{si} and A_{si} denote the modulus of elasticity and area of steel bar i; E_{bi} is the modulus of elasticity of the bond interface of bar i; and ρ_{bi} is the perimeter of bar i.

3.3.1. *Fiber-Section Model*

To determine Eq. (16), a common technique involves subdividing the frame section into fibers (layers), as illustrated in Fig. 3, to establish the nonlinear relationship between frame-section forces and deformations. Each fiber (layer) shows a constitutive material of the frame section. This technique, known as the "*fiber-section model*," was introduced and described by Spacone and Limkatanyu [26]. It inherently considers the coupling effects between frame axial force and bending moment. In this study, we utilize this technique to refine the element cross-section. As a result, Eq. (16) need to be modified and can be expressed as [42]:

$$\mathbf{k}_F = \begin{bmatrix} \sum_{j=1}^{j=nfib} E_j^{fib} A_j^{fib} & \sum_{j=1}^{j=nfib} -y_j E_j^{fib} A_j^{fib} & \vdots & 0 & \cdots & 0 \\ \sum_{j=1}^{j=nfib} -y_j E_j^{fib} A_j^{fib} & \sum_{j=1}^{j=nfib} y_j^2 E_j^{fib} A_j^{fib} & \vdots & 0 & \cdots & 0 \\ \cdots & \cdots & \cdots & \cdots & \cdots & \cdots \\ 0 & 0 & \vdots & E_{s1}A_{s1} & \cdots & 0 \\ \cdots & \cdots & \vdots & \cdots & \cdots & \cdots \\ 0 & 0 & \vdots & 0 & \cdots & E_{sn}A_{sn} \end{bmatrix} \quad \text{and} \quad \mathbf{k}_b = \begin{bmatrix} E_{b1}\rho_{b1} & \cdots & 0 \\ \cdots & \cdots & \cdots \\ 0 & \cdots & E_{bn}\rho_{bn} \end{bmatrix} \tag{17}$$

where *nfib* is the number of fibers in the RAC frame section; and *j* represents a generic fiber. It is important to note that the elastic modulus of each material in Eq. (17) depends on the state of deformation according to each material model, as presented in Sec. 4.

Based on the fiber-section model [26], the frame and bond-interface forces can be rewritten as follows [42]:

$$\mathbf{D}(\mathbf{x}) = \left\{ \sum_{j=1}^{j=nfib} \sigma_j^{fib} A_j^{fib} \quad \sum_{j=1}^{j=nfib} -y_j \sigma_j^{fib} A_j^{fib} \quad \bar{\sigma}_{s1} A_{s1} \quad \cdots \quad \bar{\sigma}_{sn} A_{sn} \right\}^T \quad \text{and} \quad \mathbf{D}_b(\mathbf{x}) = \{D_{b1}(x) \quad \cdots \quad D_{bn}(x)\}^T \tag{18}$$

where σ_j^{fib} is the normal stress of fiber *j*; $\bar{\sigma}_{si}$ and $D_{bi}(x)$ are the normal stress and bond-interface force of bar *i*.

To solve nonlinear analysis of RAC members under static loading conditions, the incremental-step solution requires linear incremental forms of the force-deformation relation for the fiber-section and bond interfaces. Thus, Eq. (14) can be given in the following incremental form [42]:

$$\mathbf{D}(\mathbf{x}) = \mathbf{D}^0(\mathbf{x}) + \Delta\mathbf{D}(\mathbf{x}) = \mathbf{D}^0(\mathbf{x}) + \mathbf{k}_F^0 \Delta\mathbf{d}(\mathbf{x}) \quad \text{and} \quad \mathbf{D}_b(\mathbf{x}) = \mathbf{D}_b^0(\mathbf{x}) + \Delta\mathbf{D}_b(\mathbf{x}) = \mathbf{D}_b^0(\mathbf{x}) + \mathbf{k}_b^0 \Delta\mathbf{d}_b(\mathbf{x}) \tag{19}$$

where the superscript 0 refers to the initial step process.

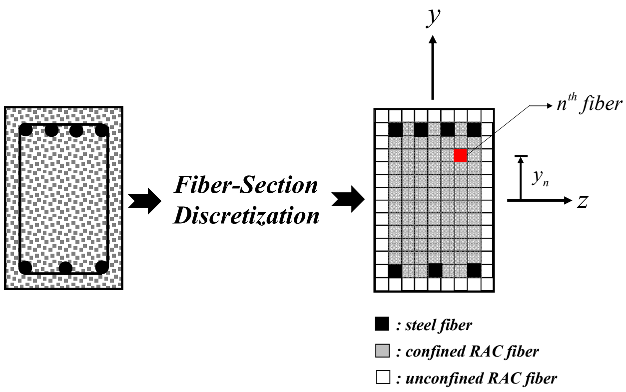

Fig. 3. Fiber-section model [49].

3.3.2. Displacement-Based Formulation

The displacement-based formulation has been widely adopted in engineering fields due to its simplicity in both formulation and implementation [48-51]. In this approach, element displacements are linked to nodal displacements through suitable displacement shape functions. Nodal displacements of the elements serve as fundamental unknowns. Frame-section deformations and bond-interface slips are determined based on frame and bond interface compatibility conditions, respectively. Hence, these are fulfilled pointwise throughout the element domain. In contrast, equilibrium conditions are satisfied only in an integral sense. This formulation can be derived using the principle of virtual displacement. As a result, the weighted residual form of equilibrium equation in Eq. (6) yields [42]:

$$\int_L \delta\mathbf{u}^{\mathrm{T}}(\mathbf{x})\left[\mathbf{L}^{\mathrm{T}}\mathbf{D}(\mathbf{x}) - \mathbf{L}_{\mathrm{b}}^{\mathrm{T}}\mathbf{D}_{\mathrm{b}}(\mathbf{x}) - \mathbf{p}(\mathbf{x})\right] = \mathbf{0} \tag{20}$$

where $\delta\mathbf{u}(\mathbf{x})$ is the kinematically admissible virtual displacement vector; and L is the element length.

By substituting the relation from Eq. (19) into Eq. (20) and incorporating the compatibility conditions of Eqs. (11) and (13), the weighted residual form of Eq. (20) can be reformulated as [42]:

$$\int_L \delta\mathbf{u}^{\mathrm{T}}(\mathbf{x})\left[\mathbf{L}^{\mathrm{T}}\left(\mathbf{D}^0(\mathbf{x}) + \mathbf{k}_{\mathrm{F}}^0(\mathbf{x})\mathbf{L}\Delta\mathbf{u}(\mathbf{x})\right) - \mathbf{L}_{\mathrm{b}}^{\mathrm{T}}\left(\mathbf{D}_{\mathrm{b}}^0(\mathbf{x}) + \mathbf{k}_{\mathrm{b}}^0(\mathbf{x})\mathbf{L}_{\mathrm{b}}\Delta\mathbf{u}(\mathbf{x})\right) - \mathbf{p}(\mathbf{x})\right] = \mathbf{0} \tag{21}$$

To transfer the order of the differential operators from the force vectors to the kinematically admissible virtual displacement vector, integration by parts is utilized in Eq. (21), yielding the following equation [42]:

$$\begin{aligned}&\int_L \left(\mathbf{L}\delta\mathbf{u}(\mathbf{x})\right)^{\mathrm{T}}\mathbf{k}_{\mathrm{F}}^0(\mathbf{x})\left(\mathbf{L}\Delta\mathbf{u}(\mathbf{x})\right)dx + \int_L \left(\mathbf{L}_{\mathrm{b}}\delta\mathbf{u}(\mathbf{x})\right)^{\mathrm{T}}\mathbf{k}_{\mathrm{b}}^0(\mathbf{x})\left(\mathbf{L}_{\mathrm{b}}\Delta\mathbf{u}(\mathbf{x})\right)dx \\ &= \delta\mathbf{U}^{\mathrm{T}}\mathbf{P} + \int_L \delta\mathbf{u}(\mathbf{x})^{\mathrm{T}}\mathbf{p}(\mathbf{x})dx - \int_L \left(\mathbf{L}\delta\mathbf{u}(\mathbf{x})\right)^{\mathrm{T}}\mathbf{D}^0(\mathbf{x})dx + \int_L \left(\mathbf{L}_{\mathrm{b}}\delta\mathbf{u}(\mathbf{x})\right)^{\mathrm{T}}\mathbf{D}_{\mathrm{b}}^0(\mathbf{x})dx\end{aligned} \tag{22}$$

where $\mathbf{U}$ denotes the element nodal displacements; and $\mathbf{P}$ is the element nodal forces.

Following the displacement-based finite element formulation [48-51], the relationship between element displacements $\mathbf{u}(\mathbf{x})$ and element nodal displacements $\mathbf{U}$ is established through appropriate displacement shape functions $\mathbf{N}(\mathbf{x})$ as follows [42]:

$$\mathbf{u}(\mathbf{x}) = \begin{Bmatrix}\mathbf{u}_{\mathrm{F}}(\mathbf{x}) \\ \bar{\mathbf{u}}(\mathbf{x})\end{Bmatrix} = \begin{Bmatrix}\mathbf{N}_{\mathrm{F}}(\mathbf{x}) \\ \mathbf{N}_{\bar{\mathrm{u}}}(\mathbf{x})\end{Bmatrix}\mathbf{U} = \mathbf{N}(\mathbf{x})\mathbf{U} \tag{23}$$

As proposed by Limkatanyu and Spacone [42], the displacement shape functions $\mathbf{N}_{\mathrm{F}}(\mathbf{x})$ and $\mathbf{N}_{\bar{\mathrm{u}}}(\mathbf{x})$ in Eq. (23) are derived from linear interpolation for axial displacement in the RAC frame and steel bars with bond-interfaces, while cubic and quadratic interpolation functions are employed for vertical displacement in the RAC frame and bond-interface slip, respectively. Consequently, these shape functions ensure C^0 and C^1 continuities for axial and transverse displacements in both the RAC frame and steel bars. Further details regarding these displacement shape functions are provided in Appendix A.

By substituting the displacement vector from Eq. (23) into Eq. (22), the weak form of the governing equations is obtained [42]:

$$\left(\int_L \begin{Bmatrix}\mathbf{B}_{\mathrm{u}}(\mathbf{x}) \\ \mathbf{B}_{\mathrm{b}}(\mathbf{x})\end{Bmatrix}^{\mathrm{T}} \begin{bmatrix}\mathbf{k}_{\mathrm{F}}^0(\mathbf{x}) & 0 \\ 0 & \mathbf{k}_{\mathrm{b}}^0(\mathbf{x})\end{bmatrix} \begin{Bmatrix}\mathbf{B}_{\mathrm{u}}(\mathbf{x}) \\ \mathbf{B}_{\mathrm{b}}(\mathbf{x})\end{Bmatrix} dx\right)\Delta\mathbf{U} = \mathbf{P} + \int_L \mathbf{N}^{\mathrm{T}}(\mathbf{x})\mathbf{p}(\mathbf{x})dx - \left(\int_L \left(\mathbf{B}_{\mathrm{u}}^{\mathrm{T}}(\mathbf{x})\mathbf{D}^0(\mathbf{x}) + \mathbf{B}_{\mathrm{b}}^{\mathrm{T}}(\mathbf{x})\mathbf{D}_{\mathrm{b}}^0(\mathbf{x})\right)dx\right) \tag{24}$$

where $\mathbf{B}_{\mathrm{u}}(\mathbf{x}) = \mathbf{L}\mathbf{N}(\mathbf{x})$ and $\mathbf{B}_{\mathrm{b}}(\mathbf{x}) = \mathbf{L}_{\mathrm{b}}\mathbf{N}(\mathbf{x})$ denote the sectional deformation-displacement matrices.

To simplify the relationship in Eq. (24), it can be reformulated into the element stiffness equation as follows [42]:

$$\left(\mathbf{K}_{\mathrm{F}}^0 + \mathbf{K}_{\mathrm{b}}^0\right)\Delta\mathbf{U} = \left(\mathbf{P} + \mathbf{P}_{\mathrm{p}}\right) - \mathbf{P}_{\mathrm{F}}^0 - \mathbf{P}_{\mathrm{b}}^0 \tag{25}$$

where,

$\mathbf{K}_{\mathrm{F}}^0 = \int_L \mathbf{B}_{\mathrm{u}}^{\mathrm{T}}(\mathbf{x})\mathbf{k}_{\mathrm{F}}^0(\mathbf{x})\mathbf{B}_{\mathrm{u}}(\mathbf{x})dx$ is the RAC frame element stiffness matrix;

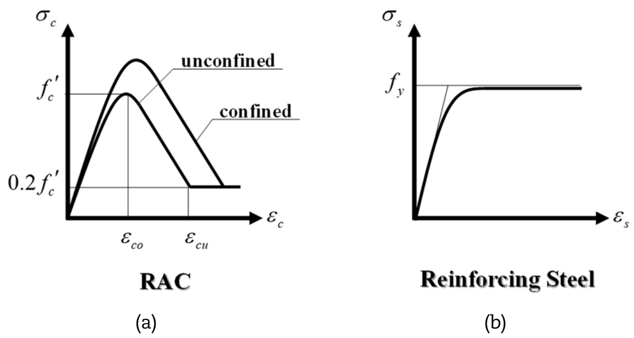

Fig. 4. Constitutive laws of: (a) RAC; and (b) steel bars [55].

$\mathbf{K}_b^0 = \int_L \mathbf{B}_b^T(\mathbf{x})\mathbf{k}_b^0(\mathbf{x})\mathbf{B}_b(\mathbf{x})dx$ is the bond-interface element stiffness matrix;

$\mathbf{P}_p = \int_L \mathbf{N}^T(\mathbf{x})\mathbf{p}(\mathbf{x})dx$ denotes the element force vector due to the distributed load vector $\mathbf{p}(\mathbf{x})$;

$\mathbf{P}_F^0 = \int_L \mathbf{B}_u^T(\mathbf{x})\mathbf{D}^0(\mathbf{x})dx$ represents the RAC frame element force vector;

$\mathbf{P}_b^0 = \int_L \mathbf{B}_b^T(\mathbf{x})\mathbf{D}_b^0(\mathbf{x})dx$ is the bond-interface element force vector.

Equation (25) illustrates the core of the displacement-based finite element formulation for the RAC frame with bond interfaces. The right-hand side of this equation represents the force residual associated with the weak statement of the equilibrium equation (Eq. (6)) and becomes zero once the equilibrium configuration is attained.

4. Constitutive Models

To describe the material behaviors of the RAC frame with bond interfaces, this study employs uniaxial constitutive laws to represent the behaviors of each component, including RAC, reinforcing steel, and bond interfaces. The details can be explained as follows:

4.1. RAC and Steel bars

In this study, the RAC model is adapted from the concrete model proposed by Kent and Park [40], which was further modified by Scott et al. [52] and Yassin [53]. This model incorporates confinement effects, tensile behavior, and damage, and is defined solely based on the normal stress, as demonstrated in the detail by Limkatanyu et al. [42]. The reinforcing steel model follows the approach of Menegotto and Pinto [41], later refined by Filippou et al. [54], incorporating isotropic hardening effects. Both models have been widely used in engineering applications to study reinforced concrete structures, and their performance in representing nonlinear responses has been confirmed [28, 48-51, 55]. The constitutive laws of RAC and steel bars are shown in Fig. 4, with further details available in the work of Limkatanyu and Spacone [27, 42], where σ_c and ε_c are the RAC stress and strain; f_c' is the RAC compressive cylinder strength in MPa; ε_{co} is the RAC strain at maximum stress in compression; ε_{cu} denotes the RAC strain at ultimate state; σ_s and ε_s are the steel bar stress and strain; and f_y represents the yield strength of steel bar.

4.2. Bond Interfaces

Bond-interface slip is a crucial factor in structural analysis, particularly in reinforced concrete structures [29-38, 55-58]. Numerous researchers have observed that bond-interface slip affects load transfer between materials, concrete crack development, structural durability, and the accuracy of structural response prediction [59-60]. In this section, experimental data from pull-out tests were collected to establish and develop the bond-interface slip law for RAC members. The details of this model are explained below:

4.2.1. Bond-Interface Stress-Slip Relation

The bond-interface stress-slip relation in this study was adapted from the bond-slip model proposed by Limkatanyu and Spacone [27, 42] and the model developed by Xiao and Falkner [29]. The bond-interface stress-slip relation is presented in Fig. 5, comprising four intervals: the initial ascending branch (OA), plateau branch (AB), and two linear descending branches (BC and CD). The bond stress corresponding to each interval can be determined from the bond slip as follows:

Region OA: $s \le s_u$

$$\tau = \tau_u \left(\frac{s}{s_u}\right)^{\alpha} \tag{26}$$

Region AB: $s_u < s \le s_p$

$$\tau = \tau_u \tag{27}$$

Region BC: $s_p < s \le s_d$

$$\tau = \tau_u - \frac{(\tau_u - \tau_d)}{s_d - s_p}(s - s_p) \tag{28}$$

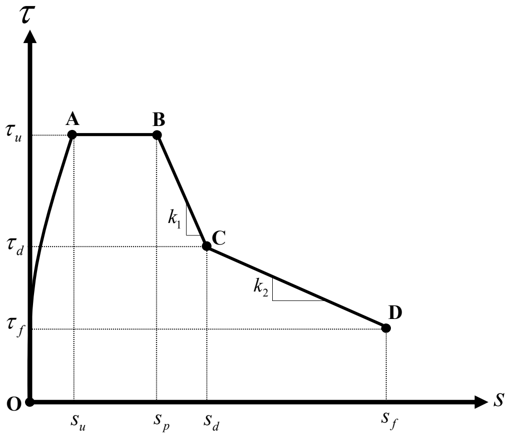

Fig. 5. Constitutive laws of bond interfaces.

Region CD: $s_d < s \leq s_f$

$$\tau = \tau_d - \frac{(\tau_d - \tau_f)}{s_f - s_d}(s - s_d) \tag{29}$$

where τ_u and s_u are the bond stress and bond slip at the maximum stress; τ_d and s_d denote the bond stress and bond slip at the first linear descending branch; τ_f and s_f represent the bond stress and bond slip at the second linear descending branch; s_p is the bond slip at the plateau branch; and α is a constant to be determined form the experimental data [29, 35, 38].

4.2.2. *Regression Analysis*

To predict each point on the bond-interface constitutive relation in Fig. 5, experimental data from a total of eighty specimens [10, 29, 30, 32, 35, 36, 61, 62] on pullout tests between RAC and steel bars were employed herein to create predicted equations based on regression analysis [43]. These specimens failed during pullout testing when a relative slip occurred between the RAC and steel bars, with no cracking observed on the surface of the RAC specimen. As reported by Su et al. [38], several factors influence the bond strength, including concrete compressive strength, steel bar diameter, RCA replacement ratio, RAC covering depth, and embedment length. In this study, these factors were used in the predicted equations to estimate parameters in the bond-interface constitutive relation, as given in Table 1.

Table 1. Proposed equation for bond-interface constitutive relation.

Parameter	Proposed equations	R^2
τ_u	$\tau_u = -1{,}995 - 2{,}625(A_s / A_c) + 244.9\sqrt{f_c'} - 0.642 f_y + \frac{c}{D}\left(33.46 - 4.129\sqrt{f_c'} - 0.0384 f_y\right) + 9{,}918\left(f_c' / f_y\right)$ $- 0.8208\left(f_y / f_c'\right)^2 - 64.88\left(f_y / f_c'\right) - 1{,}191\left(f_c^{B/2} / f_y\right)$	0.9666
s_u	$s_u = -22.1 + 0.401D + \frac{A_s}{A_c}(-2{,}061 + 184D) + 8.13\left(\tau_u / \sqrt{f_c'}\right) + \frac{D}{c}\left(160.4 - 8.46D - 26.82\left(\tau_u / \sqrt{f_c'}\right)\right) + \frac{c}{D}\left(1.355 - 0.616\left(\tau_u / \sqrt{f_c'}\right)\right)$	0.8289
s_p	$s_p = \frac{1}{f_c' A_c c D^2}\Big[-196 f_c' A_s c D^2 + A_c\left(D^3\left(81.3 f_c' - 10.17 f_y\right) + c^2\left(2.71 f_c' D - 0.391 f_y D + 8.19 f_c' s_u\right)\right.$ $\left. + c\left(D^2\left(f_y(4.01 - 0.085RCA) + f_c'(-28.9 + 0.1263D + 1.146RCA)\right) + f_c' D s_u(-45.8 + 10.66RCA) + 64.1 f_c' s_u^2\right)\right)\Big]$	0.8629
τ_d	$\tau_d = -917 - 5.15221x10^6 (A_s / A_c)^2 - 21.7(c / D)^2 + 340(c / D) - 3{,}190(D / c) + \frac{A_s}{A_c}(118{,}993 - 17{,}739(c / D) + 306{,}851(D / c))$ $+ \frac{306 f_c'^2 + \sqrt{f_c'}\tau_u\left(-53.5 f_c' - 7.94 f_y\right) + 1.97 f_y \tau_u^2}{f_c' f_y}$	0.9291
s_d	$s_d = 1.72 - 22.35(D / c) + 608(A_s / A_c) + 0.0812\left(f_y / f_c'\right)$	0.5761
τ_f	$\tau_f = 96.5 + 564\left(f_c' / f_y\right) + 5.02\tau_u - 33.63\left(\tau_u / \sqrt{f_c'}\right) + 2.076\left(\tau_u^2 / \sqrt{f_c'}\right) + \sqrt{f_c'}\left(-19.35 - 101.5\left(\tau_u / f_y\right)\right)$	0.9601
s_f	$s_f = 50.02 + 0.1619D + \frac{f_c'}{f_y^2}\left(8{,}438 f_c' - 809 f_y\right) - 123.6(s_u / D) - 268(s_u / D)^2 - 1.421\left(\tau_u^2 / f_c'\right) +$ $+ c\left(-0.756 + 3.676(s_u / D) + 0.1281\left(\tau_u / \sqrt{f_c'}\right)\right) + \frac{-106.4 f_c' \tau_u + 7.69 f_y \tau_u}{\sqrt{f_c'} f_y}$	0.9092
α	$\alpha = 0.246 - 0.024\left(\tau_u / \sqrt{f_c'}\right)$	0.1850

Note: f_c' denotes the RAC compressive cylinder strength in MPa; f_y is the yield strength of steel bar in MPa; A_s and A_c are the cross-section area of steel bar and RAC in mm²; D is the steel bar diameter in mm; c is the covering of RAC in mm; RCA denotes the replacement ratio of RCA in the mixture; τ_u represents the bond stress at the maximum stress in MPa; and s_u is the bond-interface slip at the maximum stress in mm.

Table 2. Bond strength models.

Authors	Equation	R^2	Reference
Proposed model	$\tau_u = -1{,}995 - 2{,}625(A_s / A_c) + 244.9\sqrt{f_c'} - 0.642 f_y + \frac{c}{D}\left(33.46 - 4.129\sqrt{f_c'} - 0.0384 f_y\right)$ $+ 9{,}918(f_c'/f_y) - 0.8208(f_y / f_c')^2 - 64.88(f_y / f_c') - 1{,}191(f_c^{\beta/2} / f_y)$	0.9666	-
CEB-FIP MC90	$\tau_u = 2.5\sqrt{f_c'}$	0.1860	[63]
Australian standard 3600	$\tau_u = 0.265\sqrt{f_c'}\left(\frac{c}{D} + 0.5\right)$	0.1333	[64]
Orangun et al.	$\tau_u = 0.083045\sqrt{f_c'}(1.2 + 3(c/D) + 50(D/l_a))$	0.1894	[65]
Wardeh et al.	$\tau_u = \sqrt{f_c'}\left[\frac{-0.33 + 0.4(c/D) + 9.5(D/l_a)}{1 + 0.125\text{RCA}}\right]$	0.1941	[36]
Seara-Paz et al.	$\tau_u = 2.5\sqrt{f_c'}(1 - 0.124\text{RCA})$	0.1409	[66]

Note: f_c' denotes the RAC compressive cylinder strength in MPa; f_y is the yield strength of steel bar in MPa; A_s and A_c are the cross-section area of steel bar and RAC in mm^2; D is the steel bar diameter in mm; c denotes the covering of RAC in mm; RCA represents the replacement ratio of RCA in the mixture; l_a is the embedded bar length in mm; τ_u is the bond stress at the maximum stress in MPa; and s_u denotes the bond-interface slip at the maximum stress in mm.

To demonstrate the accuracy of the proposed equations in Table 1, available bond strength models from literature [36, 63-66] were compared, as shown in Table 2 and Fig. 6. Table 2 illustrates that each bond strength model was established based on different assumptions and factors, resulting in various forms. The comparison results in Fig. 6 indicate that the proposed model is the most accurate, achieving an R^2 value of 0.9666 for this study. This can be attributed to the fact that the proposed model accounts for all factors influencing bond strength. Therefore, this provides evidence of the accuracy of the proposed equation compared to previous models.

4.2.3. *Validation of Bond-Interface laws*

In addition to the bond strength analysis in Fig. 6, this section investigates the accuracy of the proposed bond-interface constitutive model. Five pullout tests between RAC and steel bars were selected from the eighty specimens to represent the accuracy of the proposed bond-interface constitutive law. The selected experimental data include RAC100L and RAC60L from Kim et al. [32], NC-100RCA from Damrongwiriyanupap et al. [10], and A8R75-2 and A10R50-2 from Prince and Singh [35]. To assess the performance of the proposed bond-interface model in predicting the complex behavior of RAC, the bond-interface constitutive model of Alharbi et al. [67] was employed. This model [67] was established to study concrete-steel rebar bond behavior and comprises two branches: ascending and descending. The bond stress and bond slip relation of this model can be expressed as follows [67]:

Ascending branch: $s \le s_u$

$$\tau = \tau_u \left(\frac{s}{s_u}\right)^{\alpha} \tag{30}$$

Descending branch: $s > s_u$

$$\tau = \tau_u - 1.3813s + 1.3813s_u \tag{31}$$

where α denotes the modified factor with a constant value of 0.452 [67].

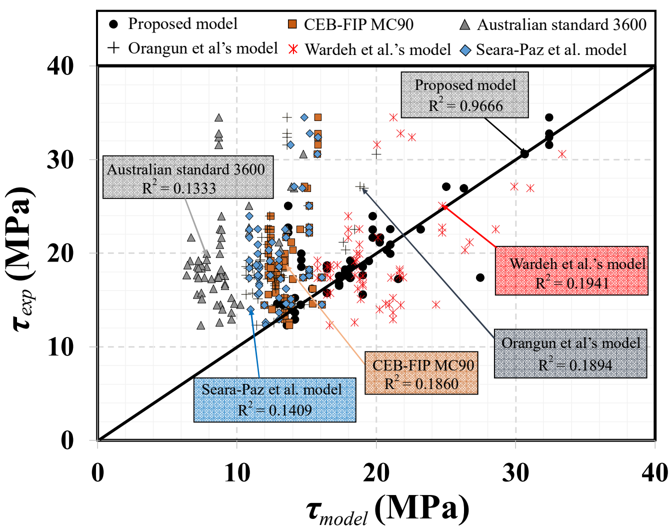

Fig. 6. Comparison of the maximum bond strength between model predictions and experiments.

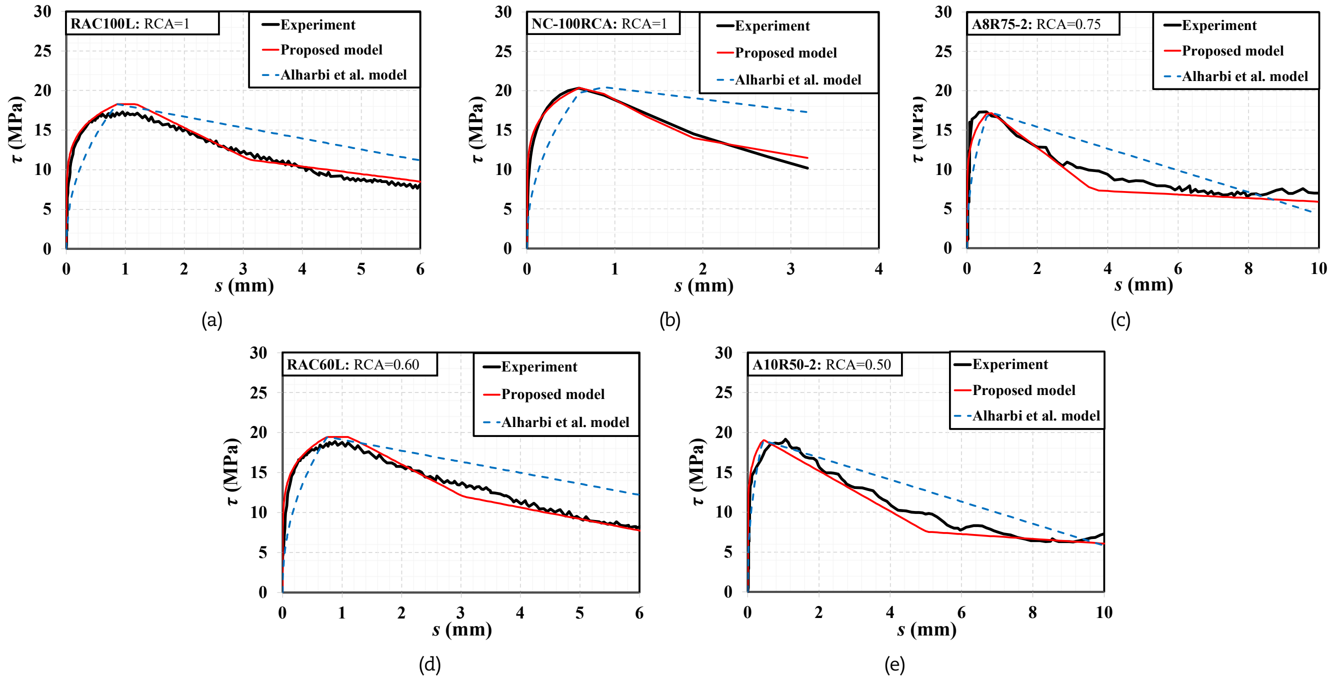

Fig. 7. Constitutive relations of: (a) RAC100L [32], (b) NC-100RCA [10], (c) A8R75-2 [35], (d) RAC60L [32], (e) A10R50-2 [35].

Figures 7(a) to 7(e) depict the bond stress and bond slip relations for five pullout test scenarios. The analytical results of the proposed model were derived from the proposed bond-interface constitutive law and the predicted equations in Table 1, while the results of the Alharbi et al. model [67] were obtained from Eqs. (30) and (31). The responses shown in Figs. 7(a) to 7(e) indicate that the proposed model effectively captures the complex behavior of the bond-interface between RAC and steel rebar, including initial stiffness, dissipated energy, maximum stress, general shape of response, and softening behavior. In contrast, the Alharbi et al. model [67] failed to predict the initial stiffness, general shape of response, and softening behavior. This can be attributed to the fact that this model comprises only two branches and was established based on limited experimental data that did not encompass all factors influencing bond-slip effects [38]. Therefore, this demonstrates the performance and accuracy of the proposed bond-interface constitutive model in predicting the bond-interface between RAC and steel bar in engineering applications.

5. Numerical Simulations

This section presents numerical simulations for RAC beams to assess and demonstrate the performance and accuracy of the proposed RAC frame model with the inclusion of the bond-interface effect. The first simulation aims to validate the accuracy of the proposed model through a convergence study, while the second simulation is focused on the impact of the bond-interface effect on beam responses. Both simulations are conducted using the general-purpose finite element platform FEAP [44]. The details of both simulations are outlined below:

5.1. Simulation I: Verification of the Proposed Model

A simply supported RAC beam system, subjected to two-point loads under the displacement control as shown in Fig. 8, is utilized to study the convergence in this work. The specimen labeled "RCA 50%," as tested by Dawood and Al-Asadi [68], is chosen to represent RAC beam responses. The material and geometric properties of the RAC beam are adopted from those proposed by Dawood and Al-Asadi [68], while the bond-interface properties are approximated using the proposed equations in Table 1. Seven Gauss-Lobatto integration points and forty discretized fibers on the cross-section are employed to analyze the RAC beam responses. This configuration has been demonstrated to be sufficient for expressing beam responses in existing literature [48-51]. It should be noted that due to the symmetry property of the RAC beam system, only half of the RAC beam is considered, as illustrated in Fig. 8.

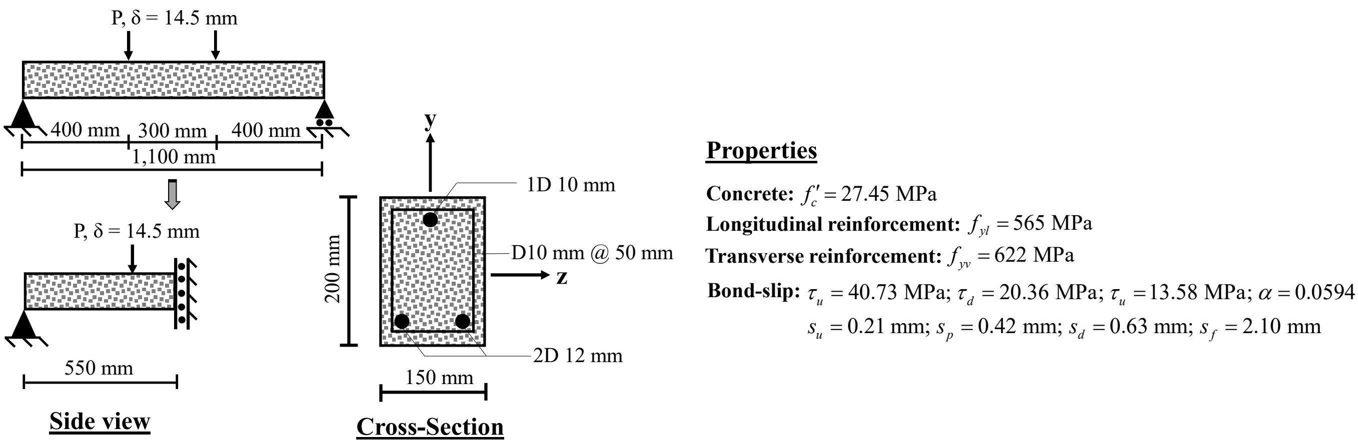

Fig. 8. Simulation I: Verification of the proposed model.

Figure 9 superimposes the applied load and midspan-displacement relationship obtained from the proposed RAC frame model with bond interface. The so-called "*benchmark*" response is established from the thirty-two proposed elements per span and used for comparison. This diagram reveals that one, two, four, and eight proposed elements per span failed to accurately represent the global load-displacement response, while sixteen proposed elements per span matched the benchmark result. The maximum load predicted by one, two, four, and eight proposed elements per span differs from the benchmark responses by approximately 33.56%, 28.11%, 17.62%, and 6.91%, respectively, while the load predicted by the sixteen proposed elements per span is slightly different by about 0.39%.

Figures 10(a) and 10(b) depict the local responses of the RAC beam model with the inclusion of bond interfaces, as derived from the proposed model. The analytical results reveal similar findings to the global response: one, two, four, and eight proposed elements per span failed to accurately demonstrate the local responses, while sixteen proposed elements per span agree well with the benchmark result (obtained from the thirty-two proposed elements per span). In particular, bending moment data jumps take place in cases where an insufficient number of elements are used, a common occurrence when employing displacement-based elements in structural models [48-51]. Additionally, as shown in Fig. 10(a), the bond-interface force and displacement at the support highlight the need a sufficient number of elements to capture the bond-slip response, even in the linear elastic region.

This simulation indicates that the number of elements is an important factor in capturing both linear and nonlinear responses of RAC structures with the inclusion of bond interfaces. The minimum number of elements required to predict these behaviors is found to be 16 proposed displacement-based elements per span for this study.

5.2. Simulation II: Impact of Bond-Interface Slip

This simulation is focused to describe the impact of bond-interface effects on the responses of the RAC beam system. The simply supported RAC beam system, labeled "RCA 70%," is used for this study. This RAC beam was previously tested by Dawood and Al-Asadi [68], resulting in the material and geometric properties shown in Fig. 11. The material properties of the bond interface are obtained from the proposed equations in Table 1. The RAC, steel bars, and bond interface models described in Section 4 are employed to represent the material behaviors of this RAC beam system. To analyze the RAC beam responses, seven Gauss-Lobatto integration points and forty discretized fibers on the cross-section are implemented in each proposed element. A total of sixteen elements per span are used to evaluate the beam responses, as determined in the previous simulation. Furthermore, two analytical models are compared to determine the influence of bond-interface slip effects relative to experimental data [68]: the proposed model with bond-slip and without bond-slip. The former considers bond-interface effects, while the latter does not account for this effect. Based on the symmetry property of the RAC beam system, only half of the RAC beam is considered, as illustrated in Fig. 11.

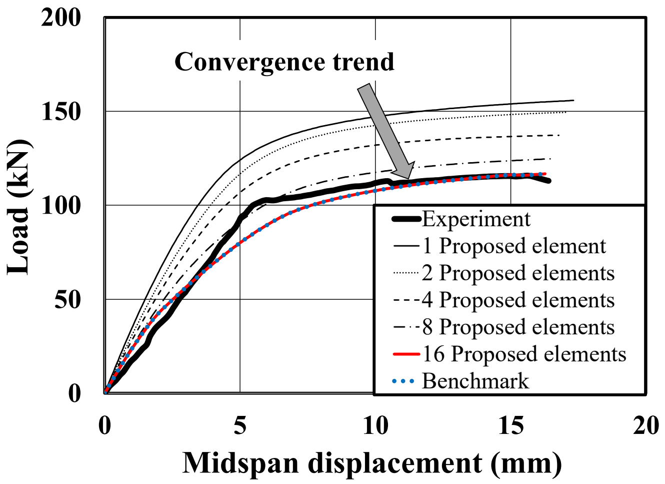

Fig. 9. Load-displacement at midspan of Simulation I.

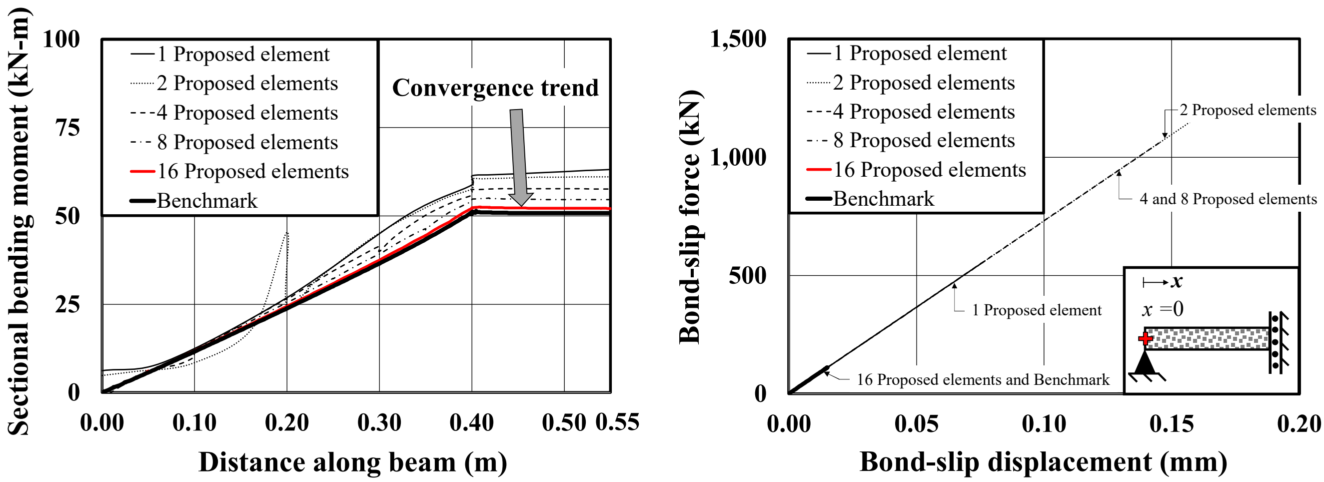

(a) (b)

Fig. 10. Local responses of Simulation I: (a) bending moment and distance along beam; and (b) bond-interface force-displacement relation.

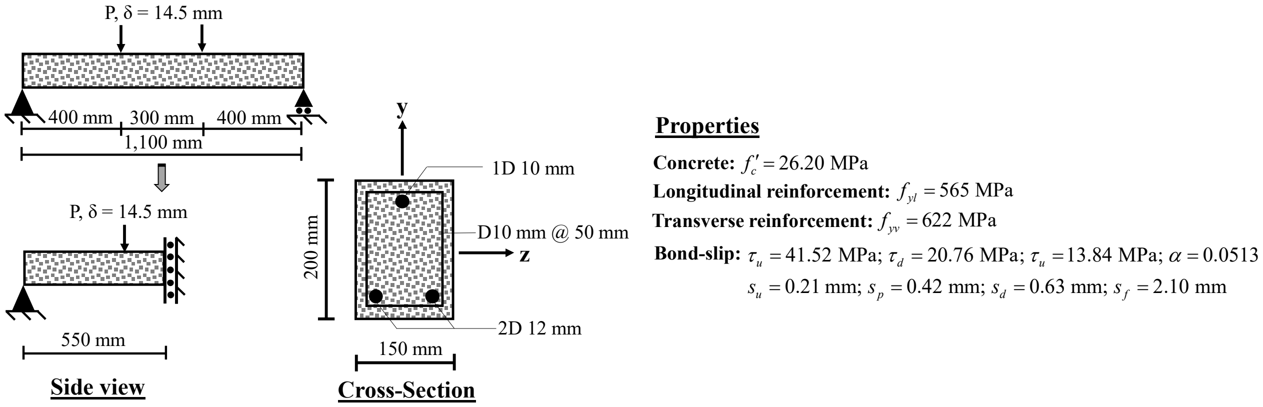

Fig. 11. Simulation II: Impact of bond-interface slip.

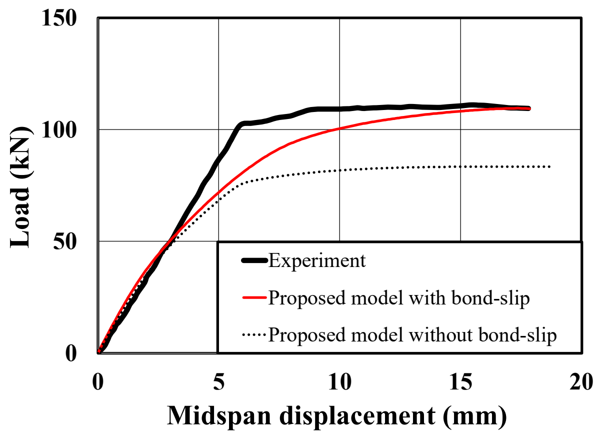

Fig. 12. Load-displacement at midspan of Simulation II.

Figure 12 presents the applied load-midspan displacement relation of the RAC beam system derived from the proposed model and compared to the experimental data. This diagram reveals that bond-interface slip leads to the weakening of the beam system stiffness, resulting in an increase in the applied load. This softening phenomenon caused by the bond-slip interface has been proven and demonstrated in several works [26, 28, 42, 60]. Consequently, the model without bond-slip predicts a maximum load differing from the experimental data by approximately 24.86%, while the model accounting for bond-slip differs from the experiment by only approximately 1.36%. Although the initial stiffness of both proposed models is slightly different, the development of applied load diverges after the plastic hinge formed at a midspan displacement of about 7.33 mm (for the model with bond-slip) and 5.56 mm (for the model without bond-slip). While the proposed model successfully captures the initial stiffness and maximum load of this RAC beam system, it fails to fully capture the general shape of the load-displacement response, likely due to the adaptation of the RAC model from the concrete model of Kent and Park [40]. In addition, several effects on the RAC beam system, such as the anchorage effect [34, 60], interfacial transition zone (ITZ) [10, 69], and confinement effect [70-71], are observed in the experiment but beyond the scope of this study.

In Fig. 13(a), the sectional bending moment along the RAC beam is compared, as obtained from the proposed models, with and without the bond-interface effect. Similar to the findings in the global response shown in Fig. 12, the bond-interface effect leads to a weakening of the system stiffness, resulting in a larger maximum bending moment for the model with bond-slip. Specifically, the maximum bending moment of the model with bond-slip is approximately 48.08% larger than that obtained from the model without bond-slip.

Figure 13(b) presents the relationship between bond-slip force and bond-slip displacement at the support. This response is observed only in the model with bond-slip, while the model without bond-slip does not account for this effect. It can be noticed from this diagram that only a linear position in the bond-interface constitutive law is demonstrated for this particular case study. This emphasizes the fact that bond-interface slip in structures occurs minimally compared to other responses. However, although the bond interface is only in the linear region, its influence seems more pronounced in other beam responses, as presented in Figs. 12 and 13(a).

From this simulation, it can be concluded that the bond-interface effect is an important factor in capture and representation of the mechanical characteristics of RAC structure systems. This effect leads to the weakening of the structural system stiffness, resulting in larger sectional forces. Therefore, it is necessary to take account of this influence in the analysis of RAC structures.

6. Conclusion

This paper introduced a novel frame model incorporating bond-interface effects for the analysis of RAC beams. The model was formulated based on the kinematic assumption of the Euler-Bernoulli beam theory and a displacement-based approach. A fiber-section model was presented, and uniaxial material models represent the behaviors of RAC, steel bars, and bond-interface slip. The RAC model was adapted from Kent and Park's concrete model [40], while the steel bars followed the model by Menegotto and Pinto [41]. A bond-interface model was proposed based on experimental data and regression analysis. Two numerical simulations were used to validate the proposed model's accuracy and applicability to RAC beam systems. From the results of this study, the following conclusions can be drawn:

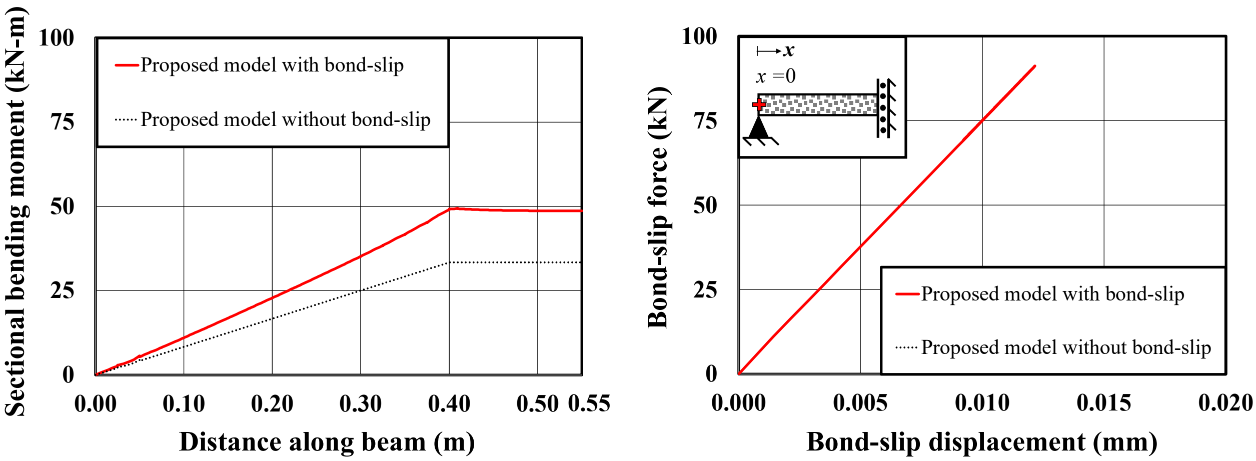

(a) (b)

Fig. 13. Local responses of Simulation II: (a) bending moment and distance along beam; and (b) bond-interface force-displacement relation.

- The proposed equations for bond strength were compared with existing literature models, demonstrating the highest accuracy with an R^2 value of 0.9666, indicating superiority over previous models.
- The proposed model accurately predicts the bond interface between RAC and steel rebar in engineering applications, capturing complex behaviors such as initial stiffness, dissipated energy, maximum stress, general response shape, and softening behavior. In contrast, the Alharbi et al. model [67], based on limited experimental data, fails to predict these factors. The performance and accuracy of the proposed model shows its promising potential for use in engineering applications.
- The first numerical simulation indicates the remarkable importance of the number of elements in predicting both global and local responses of RAC structures, highlighting the necessity of employing a minimum of 16 proposed displacement-based elements per span for this study.
- The second simulation concludes that the bond-interface effect is crucial for capturing and representing the mechanical characteristics of RAC structure systems. This effect weakens the structural system stiffness, leading to larger sectional forces. Hence, it is imperative to consider this influence in the analysis of RAC structures.

The next step in developing the proposed RAC model with the bond-slip interface is to consider the interaction effect between the structure and foundation. This will be useful for the analysis of structural systems on foundations, which is extensively applied in the engineering field.

Author Contributions

W. Sae-Long played a role in conceptualization, methodology, data curation, software, deriving the formulation, implementing the numerical model, interpreting the numerical results, validation, writing main parts of the manuscript, revising the manuscript, project administration, and funding acquisition; S. Limkatanyu played a role in deriving the formulation, software, and supervision; N. Damrongwiriyanupap played a role in writing and revising the manuscript, validation, supervision, and funding acquisition; P. Sukontasukkul played roles in supervision and investigation; T. Phoo-Ngernkham played a role in data curation; T. Imjai and S. Keawsawasvong played roles in investigation. The manuscript was written through the contribution of all authors. All authors discussed the results, reviewed, and approved the final version of the manuscript.

Acknowledgments

The authors would like to extend their special thanks to Professor Long-yuan Li for reviewing and improving the English in this paper.

Conflict of Interest

The authors declared no potential conflicts of interest concerning the research, authorship, and publication of this article.

Funding

Financial support of this work was provided by National Research Council of Thailand (NRCT) (Grant No. N42A670090) and by University of Phayao and Thailand Science Research and Innovation Fund (Fundamental Fund 2024).

Data Availability Statements

The datasets generated and/or analyzed during the current study are available from the corresponding author on reasonable request.

References

[1] Sae-Long, W., Chompoorat, T., Limkatanyu, S., Hansapinyo, C., Damrongwiriyanupap, N., Sukontasukkul, P., Chub-Uppakarn, T., Chaowana, P., Buckling behavior of *Dendrocalamus sericeus* Munro bamboo bars: Experiments and application, *Journal of Building Engineering*, 80, 2023, 108027.
[2] Ma, Z., Zhang, Z., Hu, R., Liu, X., Shen, J., Wang, C., Chloride resistance and improvement of fully recycled cementitious materials with both recycled aggregate and recycled powder, *Journal of Sustainable Cement-Based Materials*, 13(1), 2024, 49-67.

[3] Kampala, A., Suebsuk, J., Sakdinakorn, R., Arngbunta, A., Chindaprasirt, P., Coal-biomass fly ash as cement replacement in loess stabilisation for road materials, *International Journal of Pavement Engineering*, 25(1), 2024, 2296956.
[4] Wang, J., Sha, C., Ly, S., Wang, H., Sun, Y., Guo, M., Life cycle carbon emissions and an uncertainty analysis of recycled asphalt mixtures, *Sustainability*, 15(23), 2023, 16368.
[5] Zhu, H., Liou, S.-R., Chen, P.-C., He, X.-Y., Sui, M.-L., Carbon emissions reduction of a circular architectural practice: A study on a reversible design pavilion using recycled materials, *Sustainability*, 16(5), 2024, 1729.
[6] Maurya, N., Srivastav, Y., Rawat, S., Sharma, M., Srivastava, R., Sihag, P., Shukla, B.K., Augmenting concrete performance and sustainability with recycled glass: A critical examination of material characteristics and construction applications, *AIP Conference Proceedings*, 3050(1), 2024, 040010.
[7] Ou, Y., Tian, G., Chen, J., Chen, G., Chen, X., Li, H., Liu, B., Huang, T., Qiang, M., Satyanaga, A., Zhai, Q., Feasibility studies on the utilization of recycled slag in grouting material for tunneling engineering, *Sustainability*, 14(17), 2022, 11013.
[8] Im, S., Zhou, F., Lee, R., Scullion, T., Impacts of rejuvenators on performance and engineering properties of asphalt mixtures containing recycled materials, *Construction and Building Materials*, 53, 2014, 596-603.
[9] Julphunthong, P., Joyklad, P., Manprom, P., Chompoorat, T., Palou, M.-T., Suriwong, T., Evaluation of calcium carbide residue and fly ash as sustainable binders for environmentally friendly loess soil stabilization, *Scientific reports*, 14, 2024, 671.
[10] Damrongwiriyanupap, N., Srikhamma, T., Plongkrathok, C., Phoo-ngernkham, T., Sae-Long, W., Hanjitsuwan, S., Sukontasukkul, P., Li, L.-Y., Chindaprasirt, P., Assessment of equivalent substrate stiffness and mechanical properties of sustainable alkali-activated concrete containing recycled concrete aggregate, *Case Studies in Construction Materials*, 16, 2022, e00982.
[11] Monika, F., Prayuda, H., Putri, W.P.A.P., Saputro, I., Luthanzah, T.R., Influence of mixed recycled coarse aggregate on the engineering properties of recycled aggregate concrete, *Journal of Building Pathology and Rehabilitation*, 8, 2023, 102.
[12] Xiao, J., Cheng, Z., Zhou, Z., Wang, C., Structural engineering applications of recycled aggregate concrete: Seismic performance, guidelines, projects and demonstrations, *Case Studies in Construction Materials*, 17, 2022, e01520.
[13] Fanijo, E.O., Kolawole, J.T., Babafemi, A.J., Liu, J., A comprehensive review on the use of recycled concrete aggregate for pavement construction: Properties, performance, and sustainability, *Cleaner Materials*, 9, 2023, 100199.
[14] Mardani, A., Hatungimana, D., Yazici, S., Sahin, H.G., Assaad, J.J., Use of recycled mortar as fine aggregates in pavement concrete applications, *Heliyon*, 10(2), 2024, e24264.
[15] Nguyen, A.D., Dosho, Y., Performance evaluation and mix proportion design of concrete using low-quality recycled aggregate: Application for structural concrete in Vietnam, *Japan Architectural Review*, 7(1), 2024, e12417.
[16] Rashwani, A., Kadan, B., Choubi, S.S., Alhammoudi, Y., Hanein, T., Guadagnini, M., Akgul, C.M., Provis, J.L., Rebuilding Syria from the rubble: Recycled concrete aggregate from war-destroyed buildings, *Journal of Materials in Civil Engineering*, 35(4), 2023, https://doi.org/10.1061/(ASCE)MT.1943-5533.0004654
[17] Nuaklong, P., Jongvivatsakul, P., Pothisiri, T., Sata, V., Chindaprasirt, P., Influence of rice husk ash on mechanical properties and fire resistance of recycled aggregate high-calcium fly ash geopolymer concrete, *Journal of Cleaner Production*, 252, 2020, 119797.
[18] Arun, A., Chekravarty, D., Murali, K., Comparative analysis on natural and recycled coarse aggregate concrete, *Materials Today: Proceedings*, 46, 2021, 8837-8841.
[19] Patra, I., Al-Awsi, G.R.L., Hasan, Y.M., Almotlaq, S.S.K., Mechanical properties of concrete containing recycled aggregate from construction waste, *Sustainable Energy Technologies and Assessments*, 53, 2022, 102722.
[20] Zhong, C., Tian, P., Long, Y., Zhou, J., Peng, K., Yuan, C., Effect of composite impregnation on properties of recycled coarse aggregate and recycled aggregate concrete, *Buildings*, 12, 2022, 1035.
[21] Siempu, R., Pancharthi, R.K., Bond characteristics of concrete made of recycled aggregates from building demolition waste, *Magazine of Concrete Research*, 69(13), 2017, 665-682.
[22] Alhawat, M., Ashour, A., Bond strength between corroded steel reinforcement and recycled aggregate concrete, *Structures*, 19, 2019, 369-385.
[23] Dacic, A., Fenyvesi, O., Abed, M., An innovative approach for evaluating the quality of recycled concrete aggregate mixes, *Buildings*, 14(2), 2024, 471.
[24] Kumar, K., Kumar, P., Comparative study on durability of concrete using recycled and natural aggregate, *E3S Web of Conferences*, 405, 2023, 03018.
[25] Yu, Y., Wang, P., Yu, Z., Yue, G., Wang, L., Guo, Y., Li, Q., Study on the effect of recycled coarse aggregate on the shrinkage performance of green recycled concrete, *Sustainability*, 13, 2021, 13200.
[26] Spacone, E., Limkatanyu, S., Responses of reinforced concrete members including bond-slip effects, *Structural Journal*, 97(6), 2000, 831-839.
[27] Limkatanyu, S., Spacone, E., Reinforced concrete frame element with bond interfaces. II: State determinations and numerical validation, *Journal of Structural Engineering*, 128(3), 2002, 356-364.
[28] Sae-Long, W., Limkatanyu, S., Damrongwiriyanupap, N., Shear-flexure-interaction frame element inclusion of bond-slip effect for seismic analysis of non-ductile RC columns, *Chiang Mai Journal of Science*, 49(1), 2022, 14-26.
[29] Xiao, J., Falkner, H., Bond behaviour between recycled aggregate concrete and steel rebars, *Construction and Building Materials*, 21(2), 2007, 395-401.
[30] Kim, S.H., Lee, S.H., Lee, Y.T., Hong, S.U., Bond between high strength concrete with recycled coarse aggregate and reinforcing bars, *Materials Research Innovations*, 18, 2014, S2-278-S2-285.
[31] Li, C., Zhao, M., Ren, F., Liang, N., Li, J., Zhao, M., Bond behaviors between full-recycled-aggregate concrete and deformed steel-bar, *The Open Civil Engineering Journal*, 11, 2017, 658-698.
[32] Kim, S.-W., Yun, H.-D., Park, W.-S., Jang, Y.-I., Bond strength prediction for deformed steel rebar embedded in recycled coarse aggregate concrete, *Materials & Design*, 83, 2015, 257-269.
[33] Kim, S.-W., Park, W.-S., Jang, Y.-I., Jang, S.-J., Yun, H.-D., Bonding behavior of deformed steel rebars in sustainable concrete containing both fine and coarse recycled aggregates, *Materials*, 10(9), 2017, 1082.
[34] Guerra, M., Ceia, F., De Brito, J., Júlio, E., Anchorage of steel rebars to recycled aggregates concrete, *Construction and Building Materials*, 72, 2014, 113-123.
[35] Prince, M.J.R., Singh, B., Bond behaviour between recycled aggregate concrete and deformed steel bars, *Materials and Structures*, 47, 2014, 503–516.
[36] Wardeh, G., Ghorbel, E., Gomart, H., Fiorio, B., Experimental and analytical study of bond behavior between recycled aggregate concrete and steel bars using a pullout test, *Structural Concrete*, 18(5), 2017, 811-825.
[37] Abdulazeeza, A., Abdulkhudhur, R., Al-Quraishi, H., Bond strength behavior for deformed steel rebar embedded in recycled aggregate concrete, *Journal of Engineering and Technological Sciences*, 53(1), 2021, 210111.
[38] Su, T., Wang, C., Cao, F., Zou, Z., Wang, C., Wang, J., Yi, H., An overview of bond behavior of recycled coarse aggregate concrete with steel bar, *Reviews on Advanced Materials Science*, 60(1), 2021, 127-144.
[39] Cao, W., Lin, D., Qiao, Q., Chen, G., Jiang, W., Peng, S. Experimental study on bond-slip properties and influence factors between rebars and recycled concrete, *Ziran Zaihai Xuebao*, 5, 2017, 36-44.
[40] Kent, D.C., Park, R., Flexural members with confined concrete, *Journal of the Structural Division*, 97(7), 1971, 1964-1990.
[41] Menegotto, M., Pinto, P.E., Method of analysis for cyclically loaded reinforced concrete plane frames including changes in geometry and nonelastic behavior of elements under combined normal force and bending, *Proceeding of IABSE Symposium on Resistance and Ultimate Deformability of Structures Acted on by Well-Defined Repeated Loads*, Lisbon, 1973.
[42] Limkatanyu, S., Spacone, E., Reinforced concrete frame element with bond interfaces. I: Displacement-based, force-based, and mixed formulations, *Journal of Structural Engineering*, 128(3), 2002, 346-355.
[43] Freund, R.J., Wilson, W.J., Mohr, D.L., *Statistical methods*, Academic Press, 2010.
[44] Taylor, R.L., *FEAP: A finite element analysis program*, User manual: version 7.3, Department of Civil and Environmental Engineering, University of California, Berkeley, USA, 2000.
[45] Ling, Y., Ni, J., Antonissen, J., Hamouda, H.B., Voorde, J.V., Wahab, M.A., Numerical prediction of microstructure and hardness for low carbon steel wire Arc additive manufacturing components, *Simulation Modelling Practice and Theory*, 122, 2023, 102664.
[46] Imran, M., Wang, D., Wahab, M.A., Three-dimensional finite element simulations of fretting wear in steel wires used in coal mine hoisting system, *Advances in Engineering Software*, 184, 2023, 103499.

[47] Ghannadi, P., Khatir, S., Kourehli, S.S., Nguyen, A., Boutchicha, D., Wahab, M.A., Finite element model updating and damage identification using semi-rigidly connected frame element and optimization procedure: An experimental validation, *Structures*, 50, 2023, 1173-1190.
[48] Limkatanyu, S., Kuntiyawichai, K., Spacone, E., Kwon, M., Nonlinear Winkler-based beam element with improved displacement shape functions, *KSCE Journal of Civil Engineering*, 17, 2013, 192-201.
[49] Sae-Long, W., Limkatanyu, S., Prachasaree, W., Horpibulsuk, S., Panedpojaman, P., Nonlinear frame element with shear–flexure interaction for seismic analysis of non-ductile reinforced concrete columns, *International Journal of Concrete Structures and Materials*, 13, 2019, 32.
[50] Sae-Long, W., Limkatanyu, S., Panedpojaman, P., Prachasaree, W., Damrongwiriyanupap, N., Kwon, M., Hansapinyo, C., Nonlinear Winkler-based frame element with inclusion of shear-flexure interaction effect for analysis of non-ductile RC members on foundation, *Journal of Applied and Computational Mechanics*, 7(1), 2021, 148-164.
[51] Limkatanyu, S., Sae-Long, W., Damrongwiriyanupap, N., Imjai, T., Chaimahawan, P., Sukontasukkul, P., Shear-flexure interaction frame model on Kerr-type foundation for analysis of non-ductile RC members on foundation, *Journal of Applied and Computational Mechanics*, 8(3), 2022, 1076-1090.
[52] Scott, B.D., Park, R., Priestley, M.J.N., Stress-strain behavior of concrete confined by overlapping hoops at low and high strain rates, *ACI Journal*, 79(1), 1982, 13-27.
[53] Yassin, M.-H.M., *Nonlinear analysis of prestressed concrete structures under monotonic and cyclic loads*, Ph.D. Dissertation, Department of Civil and Environmental Engineering, University of California, Berkeley, USA, 1994.
[54] Filippou, F.C., Popov, E.P., Bertero, V.V., Effects of bond deterioration on hysteretic behavior of reinforced concrete joints, *EERC Report 83-19*, Earthquake Engineering Research Center, University of California, Berkeley, USA, 1983.
[55] Sae-Long, W., Limkatanyu, S., Hansapinyo, C., Imjai, T., Kwon, M., Forced-based shear-flexure-interaction frame element for nonlinear analysis of non-ductile reinforced concrete columns, *Journal of Applied and Computational Mechanics*, 6, 2020, 1151-1167.
[56] Lindorf, A., Curbach, M., Slip behaviour at cyclic pullout tests under transverse tension, *Construction and Building Materials*, 25(8), 2011, 3617-3624.
[57] Godat, A., Aldaweela, S., Aljaberi, H., Tamimi, N.A., Alghafri, E., Bond strength of FRP bars in recycled-aggregate concrete, *Construction and Building Materials*, 267, 2021, 120919.
[58] Phiangphimai, C., Joinok, G., Phoo-ngernkham, T., Hanjitsuwan, S., Damrongwiriyanupap, N., Sae-Long, W., Sukontasukkul, P., Chindaprasirt, P., Shrinkage, compressive and bond strengths of alkali activated/cement powder for alternative coating applications, *Construction and Building Materials*, 400, 2023, 132631.
[59] Pothisiri, T., Panedpojaman, P., Modeling of bonding between steel rebar and concrete at elevated temperatures, *Construction and Building Materials*, 27(1), 2012, 130-140.
[60] Mazumder, M.H., Gilbert, R.I., Finite element modelling of bond–slip at anchorages of reinforced concrete members subjected to bending, *SN Applied Sciences*, 1, 2019, 1332.
[61] Namarak, C., Tangchirapat, W., Jaturapitakkul, C., Bar-concrete bond in mixes containing calcium carbide residue, fly ash and recycled concrete aggregate, *Cement and Concrete Composites*, 89, 2018, 31-40.
[62] He, Z.-J., Chen, Y., Ma, Y.-N., Zhang, X.-J., Jin, Y.-X., Song, J., The study on bond-slip constitutive model of steel-fiber high-strength recycled concrete, *Structures*, 34, 2021, 2134-2150.
[63] Comité Euro-International du Béton, and the Fédération Internationale de la Précontrainte, *CEB-FIP Model Code 1990*, Thomas Telford, Lausanne, Switzerland, 1993.
[64] AS3600, *Australian Standard for Concrete Structures*, North Sydney, Australia, 1994.
[65] Orangun, C.O., Jirsa, J.O., Breen, J.E., A reevaluation of test data on development length and splices, *ACI Journal*, 12(9), 1977, 114-122.
[66] Seara-Paz, S., González-Fonteboa, B., Eiras-López, J., Herrador, M.F., Bond behavior between steel reinforcement and recycled concrete, *Materials and Structures*, 47, 2014, 323-334.
[67] Alharbi, Y.R., Galal, M., Abadel, A.A., Kohail, M., Bond behavior between concrete and steel rebars for stressed elements, *Ain Shams Engineering Journal*, 12(2), 2021, 1231-1239.
[68] Dawood, M.H., Al-Asadi, A.K., Mechanical properties and flexural behaviour of reinforced concrete beams containing recycled concrete aggregate, *Scientific Review Engineering and Environmental Sciences*, 31(4), 2022, 259-269.
[69] Gao, S., Guo, J., Zhu, Y., Jin, Z., Study on the influence of the properties of interfacial transition zones on the performance of recycled aggregate concrete, *Construction and Building Materials*, 408, 2023, 133592.
[70] de Azevedo, V.D.S., de Lima, L.R.O., Vellasco, P.C.G.D.S., Tavares, M.E.D.N., Chan, T.-M., Experimental investigation on recycled aggregate concrete filled steel tubular stub columns under axial compression, *Journal of Constructional Steel Research*, 187, 2021, 106930.
[71] Huang, L., Xie, J., Huang, J., Li, L., Lu, Z., Huang, P., Compressive behaviour of GFRP-confined geopolymeric recycled aggregate concrete: Effects of RA content, GRAC size and confinement ratio, *Engineering Structures*, 291, 2023, 116421.

Appendix A

The displacement shape functions $\mathbf{N}_{F}(\mathbf{x})$ and $\mathbf{N}_{\ddot{u}}(\mathbf{x})$ in Eq. (23) are given by Limkatanyu and Spacone [42] as follows:

$$\mathbf{N}_{F}(\mathbf{x}) = \begin{bmatrix} \mathbf{N}_{F1}(\mathbf{x}) & \vdots & \mathbf{N}_{F3}(\mathbf{x}) \\ \mathbf{N}_{F2}(\mathbf{x}) & \vdots & \mathbf{N}_{F4}(\mathbf{x}) \end{bmatrix} \tag{A.1}$$

$$\mathbf{N}_{\ddot{u}}(\mathbf{x}) = \begin{bmatrix} \mathbf{N}_{\ddot{u}1}(\mathbf{x}) \\ \vdots \\ \mathbf{N}_{\ddot{u}n}(\mathbf{x}) \end{bmatrix} \tag{A.2}$$

in which

$$\begin{aligned} &\mathbf{N}_{F1}(\mathbf{x}) = \begin{bmatrix} 1-\frac{x}{L} & 0 & 0 & 0 & \ldots \end{bmatrix};\ \mathbf{N}_{F2}(\mathbf{x}) = \begin{bmatrix} \frac{x}{L} & 0 & 0 & 0 & \ldots \end{bmatrix} \\ &\mathbf{N}_{F3}(\mathbf{x}) = \begin{bmatrix} 0 & 1-\frac{3x^2}{L^2}+\frac{2x^3}{L^3} & x-\frac{2x^2}{L}+\frac{x^3}{L^2} & 0 & \ldots \end{bmatrix};\ \mathbf{N}_{F4}(\mathbf{x}) = \begin{bmatrix} 0 & \frac{3x^2}{L^2}-\frac{2x^3}{L^3} & \frac{x^3}{L^2}-\frac{x^2}{L} & 0 & \ldots \end{bmatrix} \end{aligned} \tag{A.3}$$

For the i[th] with the bond-interface:

$$\begin{array}{l} \phantom{\mathbf{N}_{\ddot{u}1}(\mathbf{x}) = \Big[0 \cdots} U_{3+i}^{1} \qquad\qquad\qquad U_{3+i}^{2} \\ \mathbf{N}_{\ddot{u}1}(\mathbf{x}) = \begin{bmatrix} 0 & \cdots & 1-\frac{x}{L} & \cdots & \vdots & 0 & \cdots & \frac{x}{L} & \cdots \end{bmatrix} \end{array} \tag{A.4}$$

where U_{3+i}^{1} denotes the nodal displacement at node 1 corresponding to the degree of freedom of 3+i, and U_{3+i}^{2} denotes the nodal displacement at node 2 corresponding to the degree of freedom of 3+i.

ORCID iD

Worathep Sae-Long https://orcid.org/0000-0001-8149-4409
Suchart Limkatanyu https://orcid.org/0000-0002-4343-7654
Nattapong Damrongwiriyanupap https://orcid.org/0000-0001-7280-5957
Piti Sukontasukkul https://orcid.org/0000-0002-9580-7063
Tanakorn Phoo-Ngernkham https://orcid.org/0000-0003-2836-604X
Thanongsak Imjai https://orcid.org/0000-0002-3220-7669
Suraparb Keawsawasvong https://orcid.org/0000-0002-1760-9838

How to cite this article: Sae-Long W., et al., Bond-Slip Model for Finite Element Analysis of Reinforced Recycled Aggregate Concrete Frames, *J. Appl. Comput. Mech.*, 11(2), 2025, 451-466. https://doi.org/10.22055/jacm.2024.46464.4532